Available online at www.sciencedirect.com
ScienceDirect
Journal of the European Ceramic Society 31 (2011) 1685–1694
www.elsevier.com/locate/jeurceramsoc

Alumina plasma spraying on 304L stainless steel: Role of a wüstite interlayer

F. Goutier, S. Valette *, M. Vardelle, P. Lefort

SPCTS UMR CNRS 6638, European Ceramic Center, 12 rue Atlantis, 87068 Limoges, France

Received 16 December 2010; received in revised form 6 March 2011; accepted 14 March 2011
Available online 13 April 2011

Abstract

Excellent adhesion values (>70 MPa) of alumina coatings achieved by Atmospheric Plasma Spraying (APS) were obtained on pre-oxidized stainless steel (304L), covered with a continuous layer of wüstite ($Fe_{1-x}O$) surmounted by a very thin magnetite layer. This is due to epitaxial relationships between alumina, magnetite and wüstite, as shown by Transmission Electron Microscopy (TEM), giving a "crystallographic bonding".

Keywords: Stainless steel; Alumina coatings; Atmospheric Plasma Spraying (APS); Transmission Electron Microscopy (TEM); Adhesion test

1. Introduction

In the field of the Atmospheric Plasma Spraying (APS), it is commonly accepted that poor adhesions of coatings are due to surface conditions of the substrates and presence of adsorbates and condensates on the substrates.[1] Consequently, in order to improve coatings adhesion, substrates are often

(i) grit blasted to ensure a strong mechanical bond between the impacting particles and the substrate and
(ii) pre-heated in air above around 600 K, in order to eliminate, from the surface, adsorbates and condensates.[2]

However the grit blasting is not always possible (e.g. on thin substrates) and may leave grit residues between the substrate and coating. Moreover, for APS processing on metals or alloys, pre-heating induces a superficial oxidation of the substrate, which is particularly noticeable for iron-based alloys. The characteristics of the formed oxide layers vary according to the pre-heating treatments, and the coatings on so-oxidized substrates present a very broad range of adhesion/cohesion values, with poor reproducibility.[3,4]

If oxidation is carried out in CO_2 instead of air,[5] the behaviour is very different: for instance, on low-carbon steels, pre-oxidations in CO_2 provide an excellent adhesion of alumina plasma sprayed coatings.[6] This result has been attributed to the presence of a wüstite phase $Fe_{1-x}O$ on the surface of the steel before alumina deposition. This new mode of adhesion has been called "crystallographic bonding", because the high adherences observed were due to the progressive sliding between the successive crystalline lattices from the inner alloy to the α-Al_2O_3 outer splats: alloy/wüstite/magnetite/γ-Al_2O_3/α-Al_2O_3. The chain of structural relationships so constituted develops strong bonds across the interfaces, without any properties gap.[7] This process presents also the advantage of sparing the grit-blasting step.

Recently, a study devoted to the oxidation of austenitic low-carbon stainless steel 304L (72 wt.% Fe, 18 wt.% Cr and 10 wt.% Ni), in CO_2, identified wüstite as the superficial oxide phase.[8] Hence it appeared as very interesting to confirm that such a pre-oxidation treatment of this last alloy provides also a good adhesion of alumina plasma deposits, knowing that, contrary to what was observed on C40E, the growth of wüstite on the 304L alloy was preceded by the inner formation of chromia and of iron-chromium spinel.

Thus, the aim of the present study was to achieve alumina coatings on alloy 304L pre-oxidized in CO_2, in order to test the coating adhesion and to characterize the interfacial relationships.

2. Experimental

2.1. Raw materials

2.1.1. Pre-oxidized 304L alloy

The substrates used were 304L steel plates, provided by Chaumeil S.A. (Brive, France). Their composition is given in

* Corresponding author at: University of Limoges, SPCTS UMR CNRS 6638, European Ceramic Center, 12 rue Atlantis, 87068 Limoges, France.
Tel.: +33 0555 45 75 54; fax: +33 0555 45 72 11.
E-mail address: stephane.valette@unilim.fr (S. Valette).

0955-2219/$ – see front matter © 2011 Elsevier Ltd. All rights reserved.
doi:10.1016/j.jeurceramsoc.2011.03.022

Table 1
Composition of the 304L stainless steel.

Element	C	Si	Mn	P	S	Cr	Ni	Co	Cu	N	Fe
wt.%	0.024	0.240	1.340	0.033	0.026	18.060	8.100	0.200	0.360	0.0830	71.534

Table 1. The disk-shaped samples were 25 mm in diameter and 7 mm in thickness. They were polished up to SiC papers grit 4000.

For the pre-oxidation treatment, they were dived during 1–60 min in the hot area of a furnace, heated by $MoSi_2$ resistors, and working in a controlled atmosphere of carbon dioxide (Air Liquide France, N27, purity of 99.7 vol.%). The gas pressure was 10^5 Pa and the temperature 1273 K. At the end of the treatment, the samples were rapidly removed out of the warm zone of the furnace.

The oxide scale has been studied exhaustively.[8] A schematic representation of its morphology is given in Fig. 1.

The outer oxide is constituted of wüstite (with traces of Fe_3O_4 at the extreme surface[9]) while the inner oxide is composed of a thin layer of chromia (at the interface substrate/oxide). A spinel phase type chromite is present inside the oxide layer, surrounding residual metallic nodules. The substrate, near the oxide, is depleted in chromium. Fig. 2a provides the XRD patterns of the surface of the oxide scale, for pre-oxidation times of 10 and 50 min, where the oxide phases wüstite and spinel are identified (Fe_3O_4, in very little quantity, is detected only by XPS).

For pre-oxidation times up to 25 min, i.e. for weight gains below 0.6 mg cm^{-2}, the roughness Ra of the surfaces increased evenly from 0.031 ± 0.001 μm (surface condition of the polished non-oxidized samples) to 0.3 ± 0.2 μm. For longer durations of pre-oxidations there was no change noticeable, Ra varying randomly between 0.3 and 0.6 μm.

2.1.2. Alumina

Alumina powders (from H. C. Starck GmbH) were only composed of the α phase corundum (JCPDS file no. 1-70-5679) and their major impurities were SiO_2, Fe_2O_3 and Na_2O (each content ≤0.01 wt.%). Two batches were used:

- AMPERIT® 740.0, which had a grain size between 5 and 22 μm (named powder [+5–22]), with a trimodal repartition of the grains around 1 μm, 8 μm and 20 μm (Fig. 3a). The micrograph of Fig. 4a shows that the grains were smooth and angular, which is characteristic of a powder obtained from a fused and crushed material;

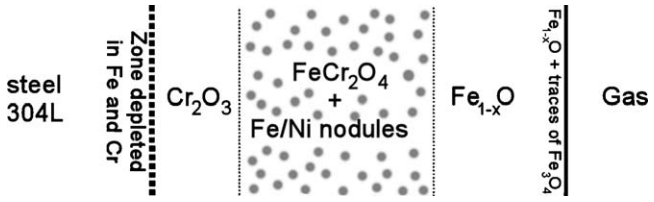

Fig. 1. Schematic cross section of the pre-oxidized stainless steel.

- AMPERIT® 740.1 with a grain size from 22 to 45 μm (named powder [+22–45]), was more homogeneous and centred around 40 μm (Fig. 3b) with some little grains around 1 μm. The aspect of the grains, seen in Fig. 4b, is the same that of the finest powder.

2.2. Plasma spraying

Thermal plasma deposition of alumina on pre-oxidized samples was carried out with a Sulzer Metco PTF4 type torch using an arc current of 600 A, with argon and dihydrogen flow rates of 33 and 10 NL min^{-1}, respectively.

Alumina powders were injected perpendicularly to the plasma jet by a powder feeder (Sulzer Metco 9MPE), through an injector of 1.5 mm diameter located at 6 mm from the nozzle exit and at 9 mm above the torch axis. Samples wheeling support (cylindrical, 120 mm in diameter) allowed 10 substrates to be treated simultaneously. In order to control the surface temperature of the substrates and eliminate particles with a too-low momentum (periphery of the jet), an air barrier was placed at

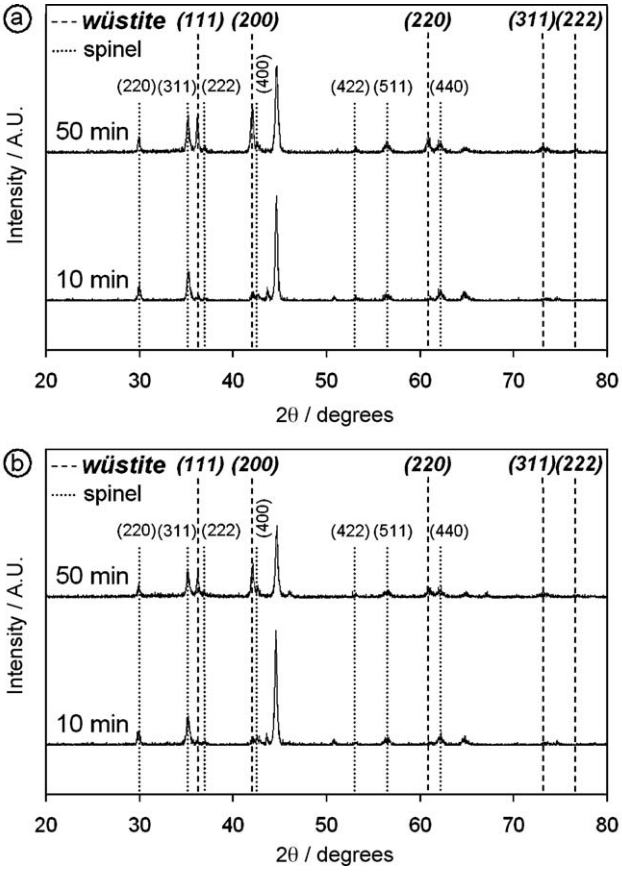

Fig. 2. XRD patterns of pre-oxidized samples before (a) and after (b) pre-heating around 600 K; the peaks not indexed are those of the substrate.

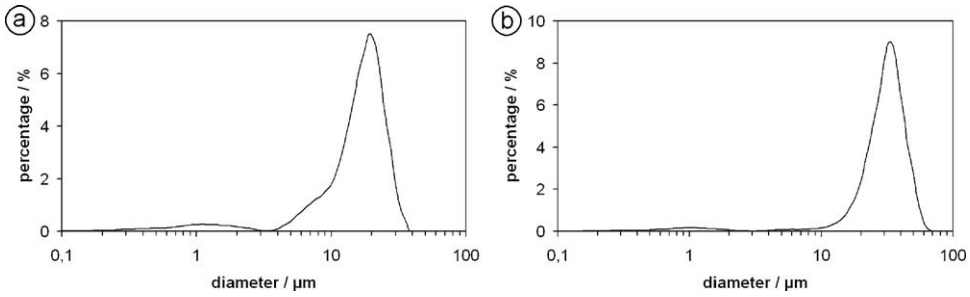

Fig. 3. Grain sizes of the powders [+5–22] (a) and [+22–45] (b).

Table 2
Particles velocity and temperature just before the impact.

	[+5–22] powder	[+22–45] powder
Impact speed (m s^{-1})	230 ± 20	240 ± 20
Impact temperature (K)	2400 ± 500	2700 ± 600

20 mm upstream of the substrates. Temperature was measured by an optical pyrometer linked to the plasma torch and focused on the sample.

For a powder mass flow rate of 20 g min^{-1}, the carrier gas flow rates were optimised at 3.5 NL min^{-1} for the powder [+22–45] and 4.5 NL min^{-1} for the powder [+5–22], using the Spray Deposit Control (SDC) device developed by SNECMA Services S.A. (Châtellerault, France) and by the SPCTS laboratory.[10] This device analyses the hot particles jet and records the substrate surface temperature (accuracy around 15%) and makes it possible to control the spray jet thermal state.

Particle temperatures and velocity were measured using the "Spray Watch" device as summarised in Table 2, for a substrate temperature around 600 K.

Deposition included several passes at the same location, in order to obtain thick coatings: the torch velocity was 250 mm s^{-1}, and 19 passes for the powder [+5–22] (or 16 passes for the powder [+22–45]) were performed in order to get an overall thickness of the alumina coatings about 260 µm.

2.3. Sample characterization

Microstructural investigations were carried out with a Scanning Electron Microscope (SEM) Philips XL 30, combined with an Energy Dispersive Spectroscopy (EDS). The phase identifications were performed with a SIEMENS D 5000 X-ray diffractometer (radiation Cu Kα, with back monochromator), operating between 2θ angles of 20° and 80° with a step of 0.02 s and an exposure time of 0.9 s. The patterns were indexed with a software DIFFRAC+ containing JCPDS data files. A Transmission Electron Microscope (TEM) study was performed with a JEOL 2010 instrument working at 200 kV and also equipped with EDS.

Adhesion of coatings was determined by following the test ASTM Standard C633-79 (1999)[11] and using a traction apparatus ADAMEL-LHOMARGY DY 26 where the samples were bonded with HTK ULTRA BOND 100® (HTK, Hamburg, Germany).

3. Results

3.1. Pre-heating treatment

Just before plasma deposition, pre-oxidized samples were pre-heated in air by the plasma jet at ca. 620 K during 90 s. This first step of the process is necessary, as seen in Section 1, for eliminating the surface adsorbates and condensates. Temperature and duration of pre-heating must be strictly limited to these values, because, for more drastic treatments, the wüstite layer completely converts into Fe_3O_4 and very brittle Fe_2O_3,[3] leading to very poor adhesions for the alumina coatings.[4]

Fig. 2b, compared to Fig. 2a shows that XRD patterns are the same before and after pre-heating, which proves that this step did not appreciably modify the composition of the surface oxides layer.

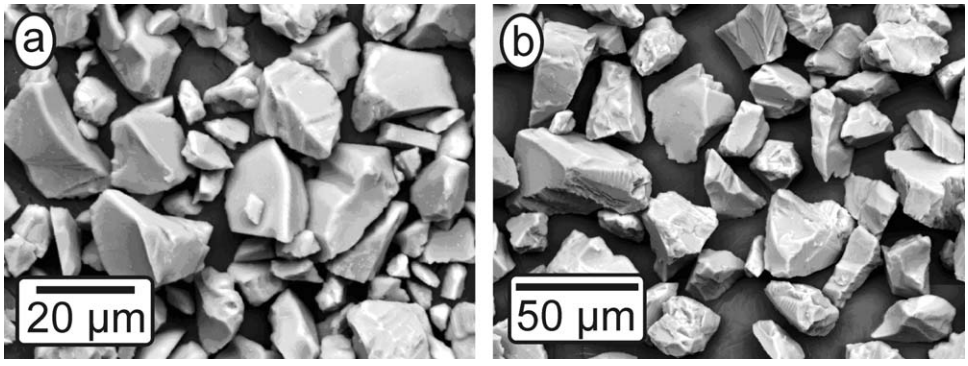

Fig. 4. SEM observation of the powders [+5–22] (a) and [+22–45] (b).

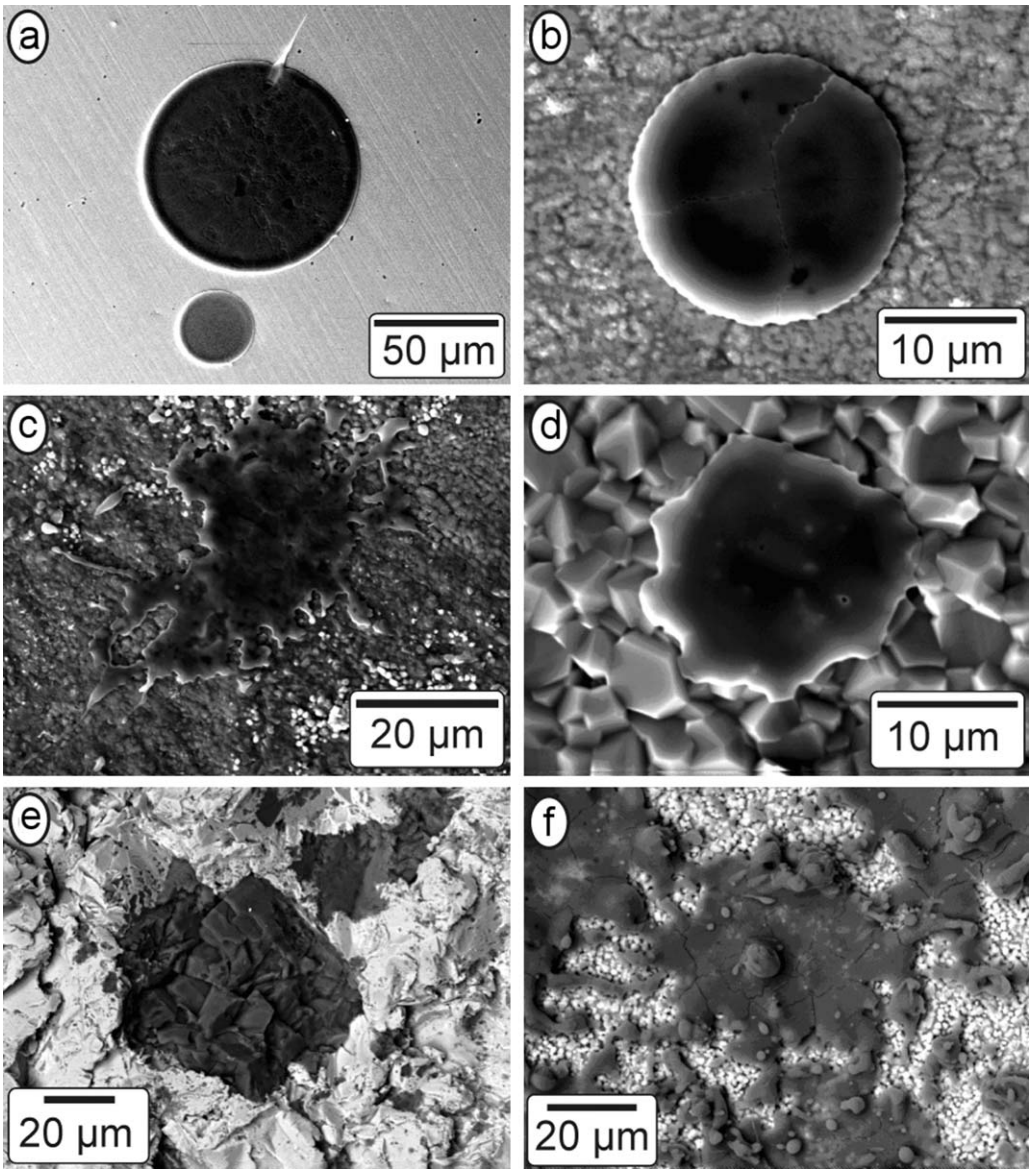

Fig. 5. Alumina splats from the powder [+5–22] on samples pre-oxidized at 1273 K in 10^5 Pa CO_2 during 1 min (a), 5 min (b), 10 min (c), 60 min (d) and on a grit blasted non-oxidized sample (e), and alumina splats from the powder [+22–45] on a sample pre-oxidized at 1273 K in 10^5 Pa CO_2 during 20 min (f).

3.2. Morphology of the coatings

Alumina splats from the powder [+5–22], deposed on not pre-oxidized samples or on weakly oxidized ones, were perfectly circular (Fig. 5a), sometimes with some micro-cracks (Fig. 5b). When a thicker oxides layer covered the surface, splashes were often observed (Fig. 5c). For the thickest oxides layers, alumina splats filled the holes of the surface (Fig. 5d) and their boundaries were angular, which is similar to the morphology observed on grit blasted samples (Fig. 5e). Splats from the powder [+22–45] presented the same shapes, with a bigger size (e.g. in Fig. 5f).

The external surface of the coatings had always the same aspect, with a juxtaposition of the last lamellae deposed, which appear as splashed and cracked on the micrographs of Fig. 6a and b for the powders [+5–22] and [+22–45], respectively.

Figs. 7a and 8a, present cross sections of samples pre-oxidized 35 min at 1273 K, respectively, for alumina [+5–22] and [+22–45]. Both powders gave the same morphology of the coatings, with a lot of pores distributed regularly and whose sizes vary approximately from 1 to 10 μm. Figs. 7b and 8b detail the interfacial zone, for the fine and coarse alumina, respectively. In fact, this zone presents always the same characteristics for the two powders and for all the pre-oxidation durations, in accordance with the schematic description of Fig. 1, but with alumina, outwards.

For comparison, if coatings on pre-oxidized samples had a microstructure similar to that of the grit blasted samples (Fig. 9a), the interfacial areas were different, with a deeper penetration of the liquid splats around the superficial asperities of the steel (Fig. 9b).

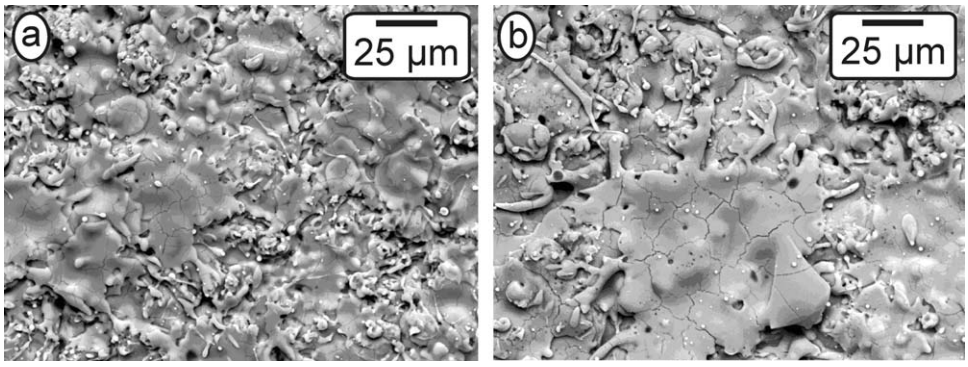

Fig. 6. Top view of the coating from the powders [+5–22] (a) and [+22–45] (b).

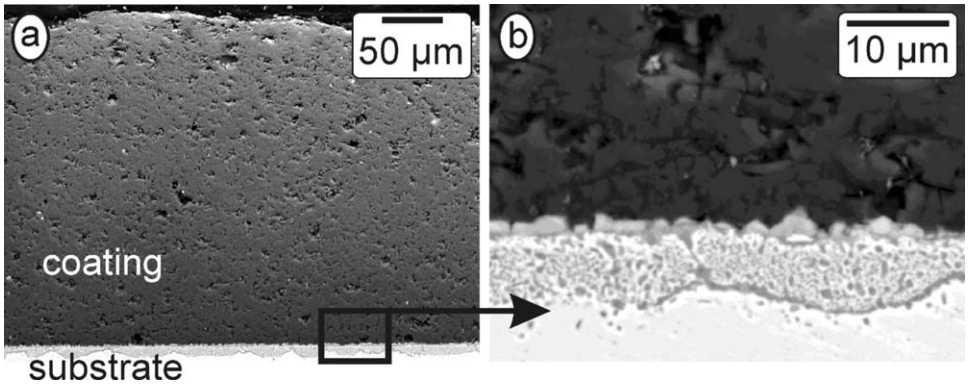

Fig. 7. Cross section of the coating from the powder [+5–22] on a sample pre-oxidized 35 min at 1273 K: overview (a) and interface detail (b).

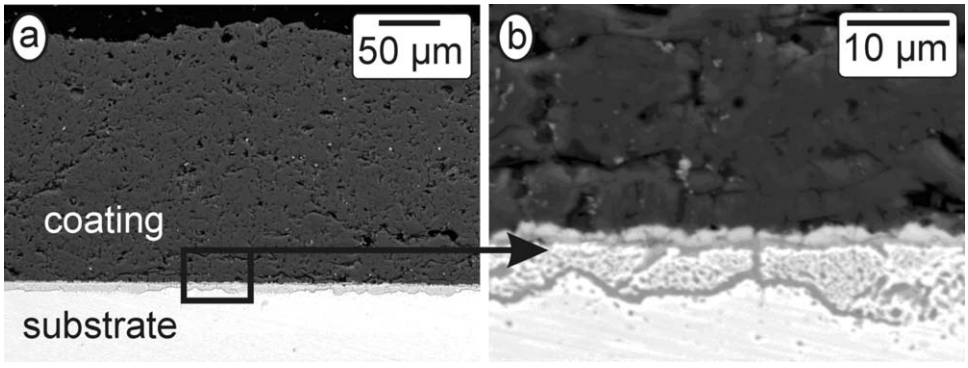

Fig. 8. Cross section of the coating from the powder [+22–45] on a sample pre-oxidized 35 min at 1273 K: overview (a) and interface detail (b).

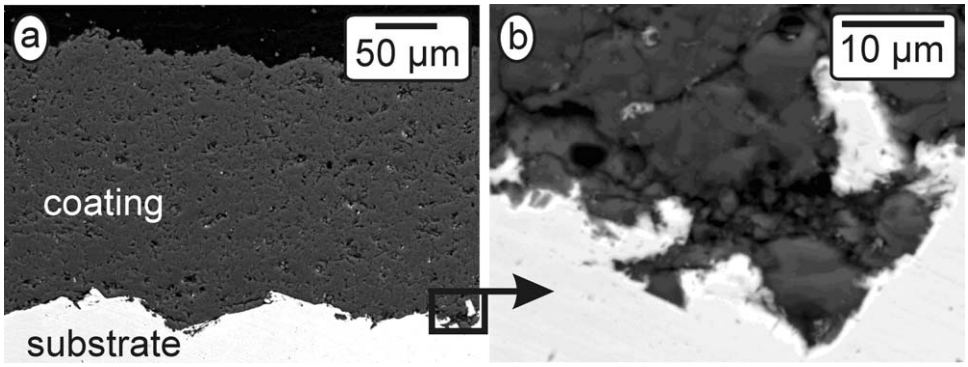

Fig. 9. Cross section of the coating from the powder [+22–45] on a grit-blasted sample: overview (a) and interface detail (b).

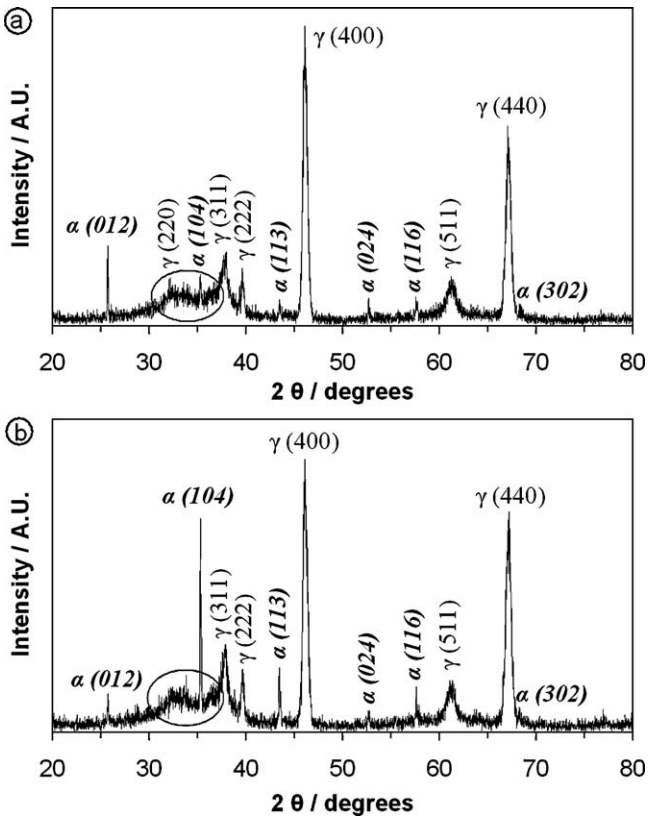

Fig. 10. X-ray diffraction patterns of the surface of coatings obtained with the powders [+5–22] (a) and [+22–45] (b).

3.3. X-ray analyses

Fig. 10a and b present the X-ray analyses of the surface of the alumina coatings achieved with the two kinds of alumina powders sprayed. They always identified the same three phases:

- the metastable cubic γ-alumina[12] that appears principally, and that is indexed with the JCPDS file no. 50-0741. Its peaks (4 0 0) and (4 4 0) are well defined and thin, by comparison with the peaks (2 2 0), (3 1 1) and (5 1 1). This difference is classically attributed to vacancies in the structure formed by the aluminium cations[12,13];
- α-alumina (corundum, JCPDS file no. 46-1212), which is the thermodynamically stable phase below 2300 K.[14] It is present in quantities much lower than γ-alumina;
- transition aluminas, poorly crystallised and in low quantities, to which the high background is attributed in the circled areas of Fig. 10a and b. In previous works, they have already been reported, after alumina thermal plasma deposition, and they are usually considered as resulting from the solid-state transformation of γ-alumina lamellae impacted by molten alumina particles.[15,16]

The difference of height of the weak peaks in the range 25–45° (2θ scale), between Fig. 10a and b, is not significant: their height varies according to the localisation of the analysis, likely due to local changes in crystals orientations, and no correlation was observed between the size of the alumina particles sprayed and the relative height of the α and γ alumina peaks (hence between the relative content of these phases[17]).

Lastly, given the great thickness of the coatings (>250 μm), it must be reminded that the X-ray analyses corresponded to the surface of the coatings and not to the interfacial area, which has been analysed specifically by Transmission Electron Microscopy (TEM) and which is presented below.

3.4. Characterization of the interfacial zone

For the characterization of the interfaces substrate/oxides and oxides/coating, thin lamellae were prepared by using samples pre-oxidized 35 min at 1273 K in 10^5 Pa of carbon dioxide (weight gain around 0.75 mg cm^{-2}), and covered by alumina [+5–22] or [+22–45]. A TEM overview of the coating obtained with the [+5–22] powder is shown in Fig. 11, where the alumina coating is in the top right, and the substrate in the bottom left.

The alumina splats have a columnar microstructure, detailed in Fig. 12a (see particularly the arrow). The associated Selected Area Electron Diffraction (SAED) patterns of Fig. 12b, where a slight diffusion along b* is visible, indicates that it is composed of γ-alumina. Indeed this diffusion is considered as due to the cationic lacunae of the lattice of γ-alumina, where vacancies and cations are more or less arranged.[13]

Another TEM micrograph (Fig. 13a) focuses on the iron oxides/alumina interface. It was obtained on a sample covered by alumina [+22–45], which is in the top right, the pre-oxidized layer being in the bottom left. Such as in Fig. 11, the contact between the iron oxides (dark) and alumina (clear) appears as perfect: this is a first sign of an excellent bonding between the alumina and the oxides layer, since the mechanical and physical treatments for thinning the TEM lamella have not separated these two phases.

Near the iron oxides/alumina interface, but inside the grains of oxide, the SAED patterns of Fig. 13b identify the f.c.c. lattice of wüstite, with diffuse spots of a superstructure, characteristic of its P′ phase, which corresponds to a composition $Fe_{1-x}O$ with $0.91 < x < 0.95$.[18]

By positioning the electron beam exactly at the iron oxide/alumina interface, the double spots observed in the SAED pattern of Fig. 13c (see arrows) clearly show two f.c.c. lattices, with parameters slightly different. They correspond to the spinel phases magnetite Fe_3O_4 and γ-Al_2O_3 with a remarkable homoaxial relationship between them, the zone axis being the same for the two oxides ([1 0 0]). The spot splitting arises as a consequence of the difference between the lattice parameters a of these compounds ($a = 0.795$ nm for γ-alumina[13] and $a = 0.839$ nm for magnetite[18]). Just below, the wüstite phase, seen on Fig. 13b exhibits again the same crystallographic orientations, considering always the [1 0 0] zone axis.

All this implies that there is a double epitaxy, in one hand between wüstite and magnetite, and in the other hand between magnetite and alumina.

Lastly, comparing Figs. 12a and 13a, the sections of the columnar grains of γ-alumina phase appeared as related to the

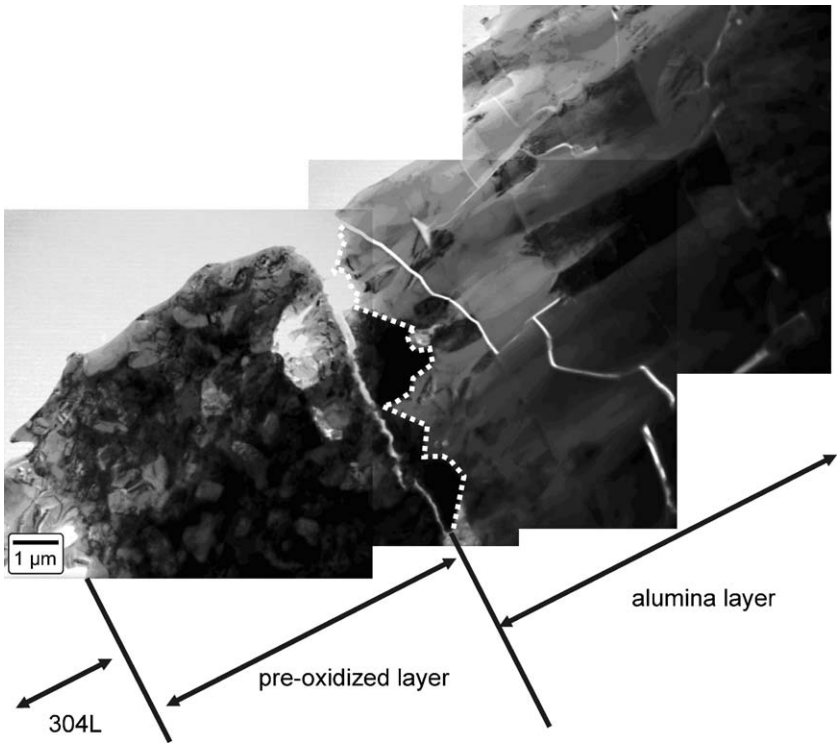

Fig. 11. TEM overview of the interfaces substrate/oxides/coating for the powder [+5–22].

grain size of the underlying iron oxide grains, and they did not depend on the size of the alumina particles deposed.

3.5. Adhesion tests

The results of the tensile adhesion tests of alumina coatings, according to the pre-oxidation time, are presented in Fig. 14 for the two powders sprayed (Fig. 14a for the [+5–22] and Fig. 14b for the [+22–45]). No significant difference appeared between them.

For samples pre-oxidized at 1273 K during less than 10 min ($\Delta m/S <$ approximately $0.2\,mg\,cm^{-2}$), the coatings had not adhered to the substrates.

One sample oxidized during 10 min precisely led to a breaking at the interface alumina/iron oxides.

For the others samples it has been impossible to quantify precisely the adhesion because the breaking always occurred in the glue, for all the tensile tests. Nevertheless, several breakings in the glue corresponding to values higher than 60 MPa, it can be deduced that adhesion of the coatings on the substrate is excellent (for one test, with a pre-oxidation of 50 min, the value reached even 73 MPa).

These results establish clearly that the good adhesion observed is due to the presence of the oxides formed during the pre-oxidation.

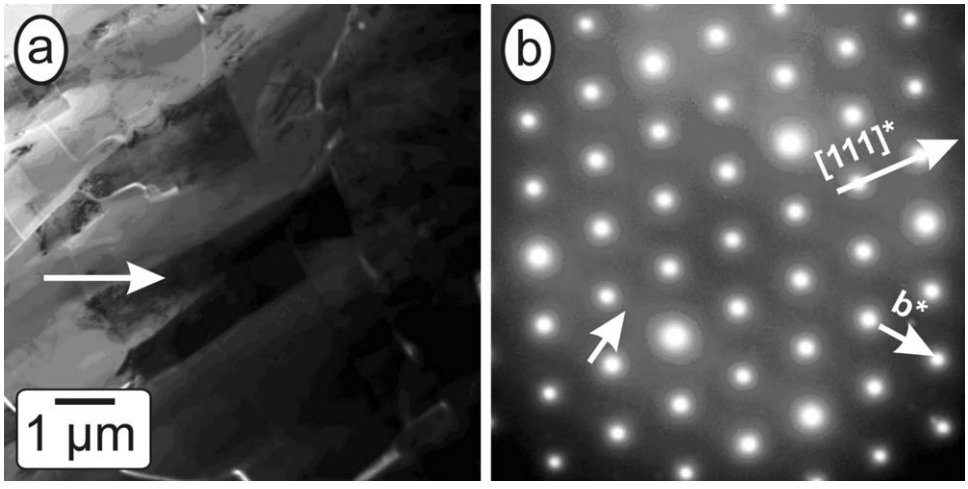

Fig. 12. Overview of the coating from the powder [+5–22] showing a columnar-type microstructure (a) and SAED pattern of the arrowed area in (a) characteristic of the γ-alumina oriented with the [1 0 0] zone axis (b).

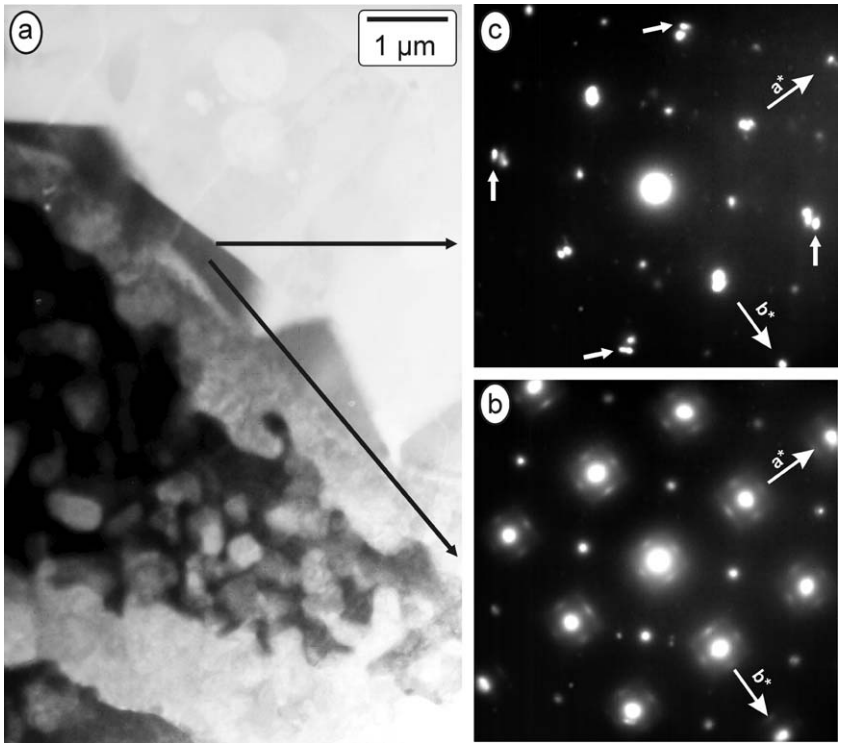

Fig. 13. Overview of the alumina/wüstite interface for a coating from the [+22–45] powder (a), SAED patterns characteristic of the P′ wüstite phase oriented with the [1 0 0] zone axis (b) and SAED patterns with the [1 0 0] zone axis at the alumina/iron oxide interface (c).

4. Discussion

The overall behaviour is identical for the two grain sizes of alumina powders used. The morphology of the coatings is the same, no difference is seen in the adhesion tests, and the same structural relationships at the interface iron oxides/alumina have been observed. This result is not really surprising, as far as the nature of the powders was the same and the impact speed also (about 230 m s^{-1}). Consequently the only difference was the grain size of the sprayed powders, which induces only two changes in the characteristics of the molten particles:

(i) their temperatures just before their impact on the substrate: the biggest were around 200 K hotter than the smallest, probably because of their thermal inertia and their slower cooling rate before their impact;
(ii) their kinetic energies of the particles at the impact, which were higher for the biggest ones.

Hence, it appeared that these two parameters (temperature and kinetic energy) were not determining in the process, the temperature being always higher than the melting point of alumina (2320 K), and the kinetic energies being suitable for the good flattening of the particles.

Now, the origin of the excellent coatings adhesion, much higher than those obtained on grit-blasted samples (30 MPa on cast iron[19]), has to be discussed. It has been seen in Section 3.5 above that it is due to the presence of the pre-oxidized layer, but this presence induces two major changes on the substrates:

(i) their roughness is much higher when they are oxidized (from 0.031 up to approximately 0.6 μm);
(ii) the chemical nature of the external phase is different: iron oxides with pre-oxidation, and alloy, without.

It has been established for long[20] that increasing the roughness of substrates enhances adhesion of coatings. As seen in Fig. 9b, on grit-blasted alloys, the liquid splats penetrate in the

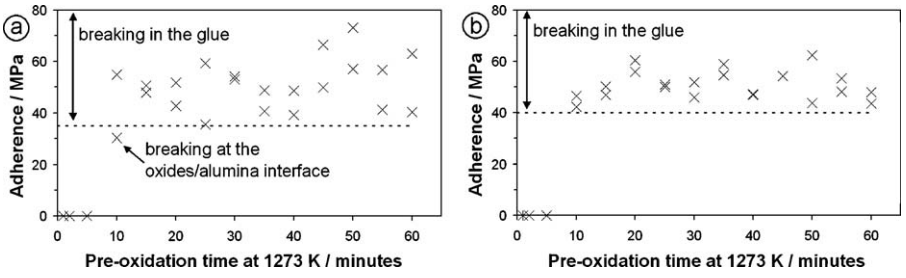

Fig. 14. Adhesion of coatings obtained with the powders [+5–22] (a) and [+22–45] (b).

holes of the surface, and so, they clasp the asperities after cooling. In the case of pre-oxidized substrates, the surface crystals are of course rough, but they do not exhibit asperities able to give joints "mortice and tenon" like, such as those of Fig. 9b. Moreover, a previous study on C40E[5] clearly showed that the thinner the wüstite layer was, the better was the coatings adhesion, hence bearing no relation with the substrate roughness.

In consequence, the increase of roughness associated to the pre-oxidation of the 304L alloy has not to be considered as being the key parameter explaining the excellent adhesion of coatings.

On the contrary, the relationship found between the oxide present at the extreme surface of the pre-oxidized 304L alloy (i.e. magnetite Fe_3O_4) and the γ-alumina deposed is exactly the same that already reported in the similar study devoted to the coating of pre-oxidized steel C40E[5] by thermal plasma spraying of alumina. The tight relationship between magnetite and γ-Al_2O_3, brought to the fore by the TEM experiments (Section 3.4 above), shows that there is no physical gap of properties when going from the iron oxide to the alumina. As far as no extra phase was detected at the interface magnetite/alumina, it means that no reaction occurred between these two phases, and hence that there was no diffusion bonding at this place.

From this, it follows that the strength of the bonding between magnetite (of the oxides scale) and alumina (of the coating) is only due to the good fitting of the crystalline lattice parameters of these two phases at their interface, called "crystallographic bonding" in previous works[6,7]: the nature of the coating adhesion is neither mechanical, nor chemical but structural.

Consequently, the presence of magnetite, even in very small quantity at the extreme surface of the pre-oxidized layer, appears as being at the origin of such a bonding. Indeed, it is likely that the crystallisation of the splats of molten alumina, in the spinel structure (γ-Al_2O_3 phase), was induced precisely by the underlying spinel arrangement of the magnetite ions, ending in the hetero-epitaxy observed.

When the substrates were insufficiently pre-oxidized ($\Delta m/S <$ approximately 0.2 mg cm^{-2}), the surface oxide was composed of chromite[8]: the absence of magnetite explains the very poor adhesion of the coatings presented in Fig. 14a and b. Otherwise, and in reference to the previous study on C40E alumina plasma coating,[6] it is likely that the thickness of the wüstite/magnetite layer plays only a little role, and, probably, it is better when it is thin.

Magnetite itself comes from the topotactic transformation of wüstite,[21] certainly favoured by the pre-heating stage: here again, there is no gap in the physical properties of the oxide scale, the crystallographic structure of the magnetite being directly derived from that of wüstite.

Beneath the wüstite scale, the composition of the solid becomes very complex as illustrated in Fig. 1. Hence, the origin of the good tensile strength of this zone remains unknown. It should need a very fine study of the relationships between the multiple phases present here: spinel-type chromite, chromine, Cr and Fe-depleted 304L alloy, and 304L bulk.

Fig. 15 (without scale) illustrates schematically the great complexity of the succession of solid phases, from the inner alloy 304L to the outer alumina.

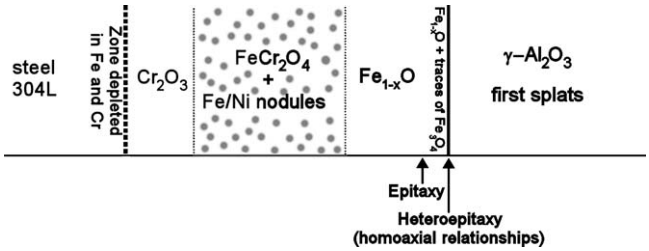

Fig. 15. Schematic representation of the continuity of the phases in the system alloy 304L/oxides/γ-alumina.

5. Conclusion

The new process of alumina coating by Atmospheric Plasma Spraying (APS) using substrates covered by a wüstite layer confirms that it provides excellent adhesions of the coatings.

The original step is the superficial formation of a wüstite phase, with magnetite Fe_3O_4 at the extreme surface, which requires a treatment of the pieces in a classical furnace, working in CO_2. The origin of the good result obtained, lies in the complex hetero-epitaxial formation of γ-Al_2O_3, when the liquid splats of alumina solidify on the substrate. This process is correlated neither with some chemical reaction (no evidence was brought about this) nor with the roughness of the substrates. The size of the molten alumina particles has no more effect on the quality of the junction, and the relative content of the α and γ alumina phase plays no role on the coatings adhesion or on their cohesion. The only reason explaining the excellent bonding observed between the substrates and their coatings, lies in crystallographic interfacial relationships, which define the "crystallographic bonding" already observed on C40E steel.

After this first study on C40E steel, and the present one, it can be thought now that such a process could be generalized for alumina coating of other iron-based alloys, provided that they could form, first, an outer layer of wüstite during a treatment of pre-oxidation.

References

1. Fauchais P. Understanding plasma spraying. *J Phys D Appl Phys* 2004;**37**:R86–108.
2. Bianchi L, Grimaud A, Blein F, Lucchese P, Fauchais P. Comparison of plasma-sprayed alumina coatings by RF and DC plasma spraying. *J Therm Spray Technol* 1995;**4**:59–66.
3. Pech J, Hannoyer B, Marest G. Duplex structure of oxides produced on low-carbon steel surfaces after DC plasma jet treatment. *Surf Coat Technol* 2000;**124**:228–34.
4. Pech J, Hannoyer B. Influence of oxide layer promoted by d.c. plasma preheating on the adhesion coating and role of the initial surface pretreatment. *Surf Interface Anal* 2000;**30**:585–8.
5. Valette S, Denoirjean A, Tétard D, Lefort P. C40E steel oxidation under CO_2: kinetics and reactional mechanism. *J Alloys Compd* 2006;**413**:222–31.
6. Valette S, Denoirjean A, Lefort P. Plasma sprayed steel: adhesion of an alumina film via a wüstite interlayer. *Surf Coat Technol* 2008;**202**:2603–11.
7. Valette S, Trolliard G, Denoirjean A, Lefort P. Iron/wüstite/magnetite/alumina relationships in plasma coated steel: a TEM study. *Solid State Ionics* 2007;**178**:429–37.

8. Goutier F, Valette S, Vardelle A, Lefort P. Oxidation of stainless steel 304L in carbon dioxide. *Corros Sci* 2010;**52**:2403–12.
9. Goutier F, Valette S, Laborde E, Lefort P. 304L stainless steel oxidation in carbon dioxide: an XPS study. *J Alloys Compd* 2011;**509**: 3246–51.
10. Renault T, Vardelle M, Fauchais P, Hoffmann H, Braillard F. On-line monitoring (SDC) through coating surface temperature of residual stresses in APS WC-Co17 wt.% coatings on Hastelloy X. In: Berndt CC, Khor KA, Lugscheider EF, editors. *Thermal spray 2001: new surfaces for a new millennium, Proceedings of the international thermal spray conference*. 2001. p. 743–50.
11. ASTM Standard C 633-79. *Standard test method for adhesion or cohesion strength of thermal spray coatings*. West Conshocken, PA, USA: ASTM International; 1999, doi:10.1520/C0633-79R99.
12. Levin I, Brandon D. Metastable alumina polymorphs: crystal structures and transition sequences. *J Am Ceram Soc* 1998;**81**:1995–2012.
13. Repelin Y, Husson E. Etudes structurales d'alumines de transition I-Alumines gamma et delta. *Mater Res Bull* 1990;**25**:611–21.
14. Barin I. *Thermochemical data of pure substances. Part I Ag–Kr, Part II La–Zr*. 2nd ed. VCH; 1993.
15. Kuroda S, Dendo T, Kitahara S. Quenching stress in plasma sprayed coatings and its correlation with the deposit microstructure. *J Therm Spray Technol* 1995;**4**:75–84.
16. Guilemany JM, Nutting J, Dougan MJ. A transmission electron microscopy study of the microstructures present in alumina coatings produced by plasma spraying. *J Therm Spray Technol* 1997;**6**:425–9.
17. Hao S, Li C-J, Yang G-J. Influence of deposition temperature on the microstructures and properties of plasma-sprayed Al_2O_3 coatings. *J Therm Spray Technol* 2011;**20**:160–9.
18. Bauer E, Pianelli A, Aubry A, Jeannot F. II—Nouvel aspect structural des wüstites métastables pures et substituées. *Mater Res Bull* 1980;**15**:323–37.
19. Krishnamurthy N, Sharma SC, Murali MS, Mukunda PG. Adhesion behavior of plasma sprayed thermal barrier coatings on Al-6061 and cast iron substrates. *Front Mater Sci China* 2009;**3**:333–8.
20. Griffiths BJ, Gawne DT, Dong G. The erosion of steel surfaces by grit-blasting as a preparation for plasma spraying. *Wear* 1996;**194**:95–102.
21. Kim BK, Szpunar JA. Orientation imaging microscopy for the study on high temperature oxidation. *Scripta Mater* 2001;**44**:2605–10.